ISSN 1063-7834, Physics of the Solid State, 2020, Vol. 62, No. 9, pp. 1534–1538. © Pleiades Publishing, Ltd., 2020.
Russian Text © The Author(s), 2020, published in Fizika Tverdogo Tela, 2020, Vol. 62, No. 9, pp. 1.370–1374.

METALS

# Parameters of the Tunnel Barrier of Superconducting Niobium-Based Structures

**M. E. Paramonov[a, *], L. V. Filippenko[a], P. N. Dmitriev[a], M. Yu. Fominsky[a], A. B. Ermakov[a], and V. P. Koshelets[a]**

[a] *Kotel'nikov Institute of Radio Engineering and Electronics, Russian Academy of Sciences, Moscow, 125009 Russia*
**e-mail: paramonov@hitech.cplire.ru*

Received March 26, 2020; revised March 26, 2020; accepted April 2, 2020

**Abstract**—The main parameters of the tunnel barrier of Josephson Nb/$AlO_x$/Nb and Nb/AlN/Nb junctions are estimated in a wide range of the current density using the Simmons method. The dependences of the tunnel barrier height and width of the resistivity are determined experimentally for each type of the junctions. A decrease in the tunnel barrier height of the junction with the AlN interlayer by 0.3 eV as compared to an oxide junction enables us to obtain the junctions with a current density higher than 15 kA/cm$^2$ at an insulating layer thickness of 10 Å allowable technologically, which gives the possibility to obtain quality parameter $R_j/R_n$ no lower than 25.

**Keywords:** superconductivity, superconducting tunnel junction, tunnel barrier parameters, Simmons method, terahertz-range receivers

**DOI:** 10.1134/S1063783420090231

## 1. INTRODUCTION

Mixers based on the superconductor–insulator–superconductor (SIS) tunnel junctions are most sensitive input elements for coherent receivers at frequencies from 0.1 to 1.2 THz: their noise temperature is only restricted by the quantum limit. Now SIS receivers are used as staff devices in most of ground-based and space radio telescopes worldwide [1–6]. To increase the operating frequency of superconducting circuits based on SIS junctions and to extend their band, high current-density tunnel junctions are necessary. However, there is the limit of enhancing the barrier transparency for alumina-based SIS junctions. This limit is 10–15 kA/cm$^2$; a further increase in the current density leads to sharp degradation of the junction quality [7–10] (Fig. 1). To overcome this limit, the technology of fabricating tunnel SIS junctions with an AlN barrier has been developed; this barrier is formed by the nitridation of an Al surface in a plasma RF discharge in a pure $N_2$ atmosphere [4–6, 10–12]. This new type of the junctions enables one to obtain the current densities higher than 15 kA/cm$^2$ for the realization of wide-band receivers and generators of the THz range. An important feature of the junctions with an AlN interlayer is the possibility to use it in combination with the top NbN electrode, which makes it possible to increase the junction gap voltage from 2.8 to 3.7 mV [10] and to increase the upper frequency boundary of operating RF devices.

## 2. METHODS OF FABRICATION OF THE TUNNEL STRUCTURES

The SIS junctions based on Nb/$AlO_x$/Nb and Nb/AlN/Nb structures were fabricated using the selective niobium etching and anodization process

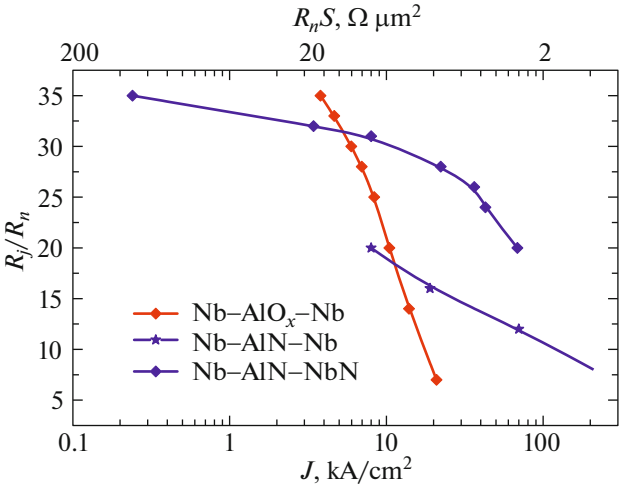


**Fig. 1.** Quality parameter $R_j/R_n$ as a function of the SIS-junction tunnel current density $J$ [10]. The values of $J$ for these junctions are calculated from the form of CVC (gap voltage $V_g$ and normal resistance $R_n$). A more universal quantity is specific resistivity of the junction $R_nS$ expressed in units Ω μm$^2$; thus, in what follows, we use the quantity $R_nS$.

(SNEAP) [13, 14]. Below we describe the process of fabricating tunnel SIS junctions developed at the Kotel'nikov Institute of Radio Engineering and Electronics of the Russian Academy of Sciences and used for the fabrication of receiving structures of the THz range [10, 15, 16]. The 24 × 24-mm silicon plates were usually used to prepare the test structures. To prevent the etching of the substrate material during the formation of the junctions by the plasma-chemical etching, a 100-nm-thick buffer stop-layer of $Al_2O_3$ was deposited by magnetron sputtering. Then we formed a photoresist mask on the substrate; the mask determined the geometry of the base electrode for the explosive lithography. The next stage is the deposition of a multilayer structure that determines the SIS-junction structure.

The deposition is performed by the magnetron sputtering during a single vacuum cycle in an ultrahigh-vacuum installation at a residual pressure of $10^{-6}$ Pa equipped with a cryogenic and turbomolecular pumps and a water-cooled substrate holder, and systems of magnetron sputtering at a direct current (DC) and at an rf frequency of 13.56 MHz. After charging the substrates in the installation and evacuating, the preliminary ionic cleaning the sample surface from organic contaminants was carried out. Then, we deposited the 200-nm-thick layer of the bottom Nb and, then, the 7-nm-thick barrier Al layer. Niobium and aluminum were deposited by the method of reactive DC deposition in an Ar atmosphere.

To obtain the barrier from aluminum oxide, the aluminum surface is oxidized in a pure oxygen atmosphere and the top Nb layer 50–100 nm in thickness is deposited. To obtain the tunnel structure with the AlN barrier, a 5–7-nm-thick aluminum layer is deposited on the 200-nm-thick bottom niobium electrode by magnetron sputtering. As shown before (for example, [17]), the thin (the thickness more than 3 nm) Al film homogeneously covers the niobium surface, preventing its oxidation. Then, a part of the aluminum layer is nitridized in the pure-nitrogen plasma; in this case, a required thickness of the tunnel barrier can be obtained by varying the discharge power and the nitridation time. A low discharge power and a large distance from the target to the sample allowed us to prevent the damage of the tunnel barrier by high-energy ions and also additional deposition of the target material during nitridation. As in the case of thermal oxidation, the remainder thin aluminum layer is superconducting due to the effect of proximity with niobium, since the coherence length in aluminum is much larger than this layer thickness. The following operation is the deposition of the top electrode from niobium or niobium nitride (NbN) 150 nm in thickness. Finally the base electrode is formed by removing the photoresist film coated by the deposited multilayer structure from the circuit portions that are not covered by the base electrode in acetone or dimethylformamide using the ultrasonics (explosive lithography).

To form the SIS-junction geometry, we used a setup of optical photolithography with a resolution of 0.7 μm, which enables one to obtain the junctions with an area less than 1 $\mu m^2$. The junctions are formed by plasma-chemical etching in the $CF_4$ medium by removing the layer of the top Nb of the multilayer structure by the photoresist mask that determines the junction geometry. The barrier $AlO_x$ or AlN layer play a role of the stop-layer that prevents further etching of the structure. After the plasma-chemical etching, the anodization is performed by the same photoresist mask, and an insulating $SiO_2$ layer with typical thickness of 250 nm is deposited by the RF-magnetron method. The anodization is necessary to provide a more reliable insulation over the SIS-junction perimeter to avoid possible shorts between the base and the top lead electrodes in these regions. The opening of the contacts to the junctions is carried out by the explosive lithography. The top lead electrode is also formed using the explosive lithography by deposition of the 300–500-nm-thick Nb layer over the photoresist mask with its subsequent removal in solvents. Similar method is used to form the regions of contact areas material of which is usually gold. The detailed description of the fabrication processes is given in [18–20].

The structures fabricated by the method described above were used when designing receiving devices for the radio astronomy [5, 6, 16], superconducting integral receivers for studying the atmosphere [21, 22], and also superconducting generators with a transmitting slot antenna [23, 24] for the transmission of the THz radiation in open space.

## 3. CALCULATION OF THE TUNNEL BARRIER PARAMETERS

To design a THz-mixer with low loss and, as a result, a low level of intrinsic noises, the capacity of a SIS junction should be compensated by the introduction of an additional inductivity. The junction capacity can be estimated after the determination of its main electrical and geometric parameters. The main characteristics of a metal–insulator–metal tunnel barrier are average barrier height $\bar{\varphi}$ and its width $d$ (Fig. 2). The characteristics of fabricated junction can be judged by these parameters. One of the parameters is the insulating layer thickness $d$ in the Nb/AlN/Nb(NbN) structures that is formed by nitriding aluminum during fabrication of a SIS mixer.

There is universal method of determination of tunnel barrier thickness $d$ and also its average height $\bar{\varphi}$ from the current–voltage characteristics (CVC) at high voltages based on the measurement of the dependence of the tunnel current density on the voltage. This dependence was proposed by Simmons [25], and

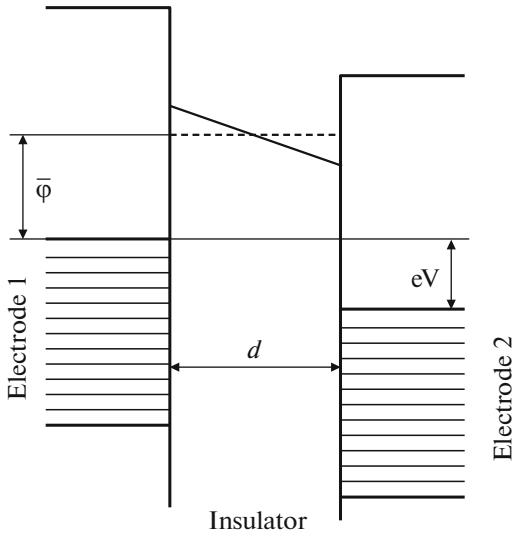


**Fig. 2.** Schematic image of the symmetric potential barrier in the tunnel junction: $\bar{\varphi}$ is the average barrier height, $d$ is the barrier width, eV is the voltage applied to the electrodes.

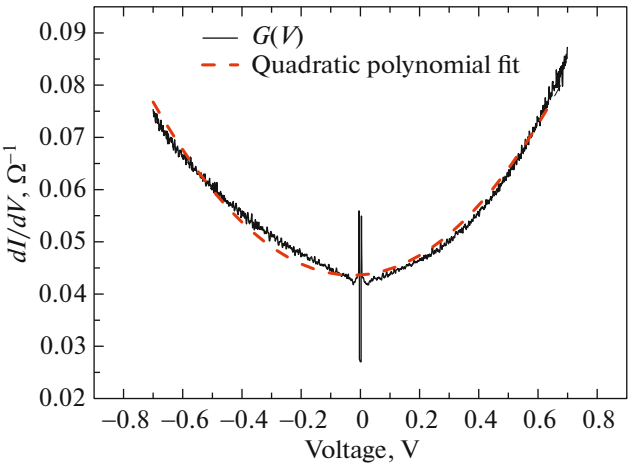


**Fig. 3.** (solid line) Dependence of the differential conductivity of the tunnel SIS junction $dI/dV$ on the voltage; (dashed line) quadratic polynomial fit.

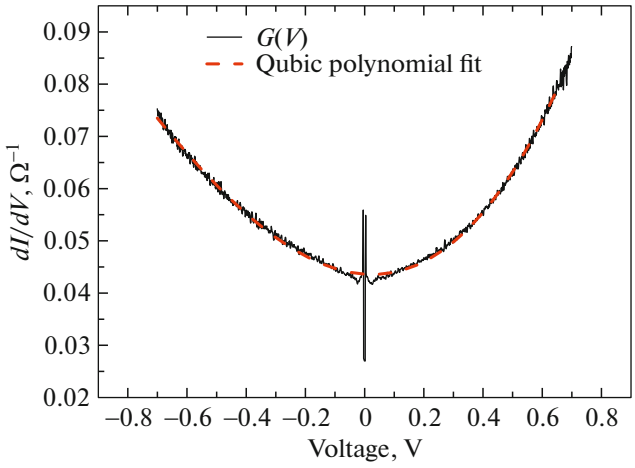


**Fig. 4.** (solid line) Dependence of the differential conductivity of the tunnel SIS junction $dI/dV$ on the voltage; (dashed line) cubic polynomial fit.

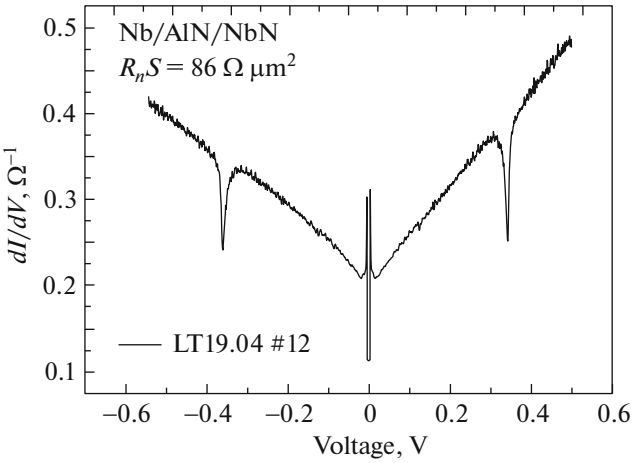


**Fig. 5.** Additional features in the characteristics of the tunnel junctions at voltages of several hundred millivolts, related to the phase slip effect or the formation of a chain of moving Abrikosov vortices in the films of the superconducting electrodes.

Brinkman [26] generalized it for tunnel junctions in the limit of low bias voltages.

It should be noted, as well, that of fundamental importance in the calculations is the parameter of the effective electron mass in the barrier that is approximately a half of the electron mass in a metal [27]. The calculation formulas and the procedure are given in detail in [28]. It is important to take into account that Eq. (2) in [28]

$$G = dI/dV = \alpha(1 + 3\gamma V^2)$$

is a simplified form of the equation

$$G(V) = \alpha + 2\beta V + 3\gamma V^2 + 4\delta V^3 + \ldots,$$

where $\alpha$, $\beta$, $\gamma$, and $\delta$ are the quantities that characterize the approximation curve in the theoretical model and they are indirectly dependent on the main parameters of the barrier. In [29], it was indicated the fact that, during processing of the experimental data and the approximation, the importance of higher degrees of $V$ in the Simmons theory increases as the range of the voltages applied to the junction increases. Using the quadratic polynomial as an approximation function

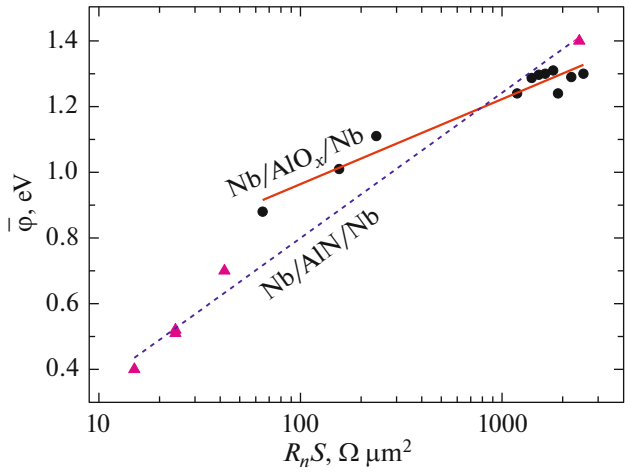


**Fig. 6.** Dependence of the tunnel barrier height on resistivity $R_nS$; points for Nb/AlO$_x$/Nb junctions, triangles for Nb/AlN/Nb junctions. The solid and dashed lines are linear approximations.

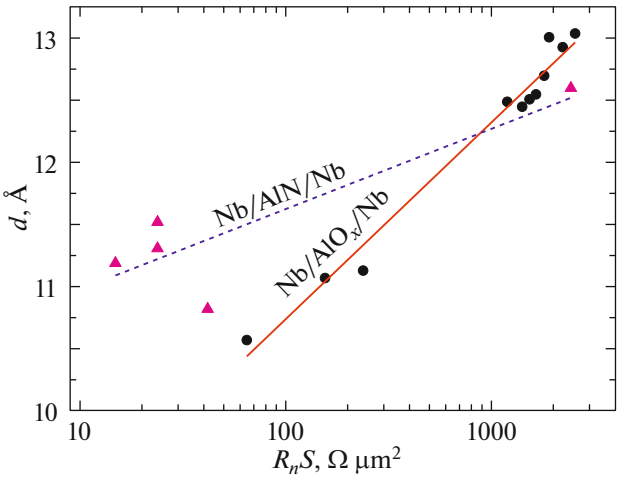


**Fig. 7.** Dependence of the tunnel barrier height on resistivity $R_nS$; points, for Nb/AlO$_x$/Nb junctions, triangles, for Nb/AlN/Nb junctions. The solid and dashed lines are linear approximations.

for the Nb/AlN/Nb junction, we obtain the theoretical curve that retraces, as a whole, the character of the curve, excepting some regions (Fig. 3).The features observed at low voltages are due to the existence of the superconducting gap.

The cubic polynomial fit gives the theoretical curve that almost completely agrees with the experimental data. The quantitative estimation of the agreement of the theory and the experimental data gives the determination coefficient for the curve of the cubic polynomial equal to 0.99 and that of the quadratic polynomial equal to 0.97 (Fig. 4). The use of such approximations enabled us to estimate parameters $\bar{\varphi}$ and $d$ more correctly, minimizing the computational error.

The dependences of $dI/dV$ on $V$ of some samples with the resistances of 10 Ω and lower demonstrate sharp dips of the conductivity at the same voltages of different polarities. Figure 5 shows, for example, curve $dI/dV(V)$ for the junction with $R_nS = 240$ Ω μm$^2$ and the resistance 3 Ω. Similar features strongly distorted the parabolic character of the curve and, sometimes, made it impossible to estimate the parameters. This phenomenon can be explained by the effect of phase slip or by the formation of a chain of moving Abrikosov vortices formed as a result of a partial breakage of the superconductivity in the films of the superconducting electrodes (low-ohmic junctions require large currents to reach a required voltage of 0.5 V).

## 4. RESULTS

The data of the calculations were used to build the dependences of the average height and the width of the tunnel junction on the resistivity $R_nS$ for two types of the barriers (Figs. 6 and 7). It is seen that the tunnel layer thickness for the AlN barrier at higher current densities (low $R_nS$) is substantially larger as compared to the oxide barrier thickness. The data for the Nb/AlO$_x$/Nb junctions were taken from [27].

It should be noted that the use of the correction for the effective electron mass in the calculations of the barrier parameters strongly influences the final result. For the AlN barrier without correction for the effective electron mass at $R_nS = 15$ Ω μm$^2$, the barrier height increases to 0.5 eV and its width decreases to 7.7 Å. The attempts to use this calculation model for the junctions with asymmetric electrodes (Nb/AlN/NbN) led to the results substantially different from the AlN barrier parameters in the Nb/AlN/Nb structures. For example, at $R_nS = 1000$ Ω μm$^2$, the barrier height was only 0.7 eV and the barrier thickness was 15.2 Å; it seems likely that the models taking into account asymmetric character of the structure should be used to correctly estimate the tunnel barrier parameters in Nb/AlN/NbN junctions. Because of this, the results obtained for the Nb/AlN/NbN junctions are not shown in Figs. 6 and 7.

## 5. CONCLUSIONS

Thus, in this work, we measured the dependences of the main parameters of the barrier on the resistivity for two types of the junctions Nb/AlO$_x$/Nb and Nb/AlN/Nb. It was shown that the low heights of the nitride barriers at a high current density (as compared to the heights of the oxide barriers) enable us to fabricate the structures with thicker barrier layers having the specific electrical conductivity no lower than 0.1 S/μm$^2$; this fact, in turn, gives the possibility of fabricating the junctions with a low leakage at the voltages lower than the gap voltage.

## FUNDING

This work was supported by the Russian Scientific Foundation, project no. 19-19-00618. The tunnel junctions were fabricated at the V. Kotel'nikov Institute of Radio Engineering and Electronics of the Russian Academy of Sciences, the state task using UNU 352529.

## CONFLICT OF INTEREST

The authors declare that they have no conflicts of interest.

## REFERENCES

1. J. R. Tucker and M. J. Feldman, Rev. Mod. Phys. **57**, 1055 (1985).
2. A. Karpov, J. Blondell, M. Voss, and K. H. Gundlach, IEEE Trans. Appl. Supercond. **5**, 3304 (1995).
3. B. D. Jackson, G. de Lange, T. Zijlstra, M. Kroug, J. W. Kooi, J. A. Stern, and T. M. Klapwijk, IEEE Trans. Microwave Theory Technol. **54**, 547 (2006).
4. A. Karpov, D. Miller, F. Rice, J. A. Stern, B. Bumble, H. G. LeDuc, and J. Zmuidzinas, IEEE Trans. Appl. Supercond. **17**, 343 (2007).
5. A. M. Baryshev, R. Hesper, F. P. Mena, T. M. Klapwijk, T. A. Van Kempen, M. R. Hogerheijde, and J. Barkhof, Astron. Astrophys. **577**, A129 (2015).
6. A. Khudchenko, A. M. Baryshev, K. I. Rudakov, P. M. Dmitriev, R. Hesper, L. de Jong, and V. P. Koshelets, IEEE Trans. Terahertz. Sci. Technol. **6**, 127 (2016).
7. R. E. Miller and W. H. Mallison, Appl. Phys. Lett. **63**, 1423 (1993).
8. A. W. Kleinsasser, R. E. Miller, W. H. Mallison, and G. B. Arnold, Phys. Rev. Lett. **72**, 1738 (1994).
9. S. K. Tolpygo, D. Yohannes, R. T. Hunt, J. A. Vivalda, D. Donnelly, D. Amparo, and A. F. Kirichenko, IEEE Trans. Appl. Supercond. **17**, 946 (2007).
10. M. Yu. Torgashin, V. P. Koshelets, P. N. Dmitriev, A. B. Ermakov, L. V. Filippenko, and P. A. Yagoubov, IEEE Trans. Appl. Supercond. **17**, 379 (2007).
11. J. Kawamura, D. Miller, J. Chen, J. Zmuidzinas, B. Bumble, H. G. LeDuc, and J. A. Stern, Appl. Phys. Lett. **76**, 2119 (2000).
12. B. Bumble, H. G. LeDuc, J. A. Stern, and K. G. Megerian, IEEE Trans. Appl. Supercond. **11**, 76 (2001).
13. H. A. Huggins and M. J. Gurwitch, Appl. Phys. **57**, 2103 (1985).
14. H. Kroger, L. N. Smith, and D. W. Jillie, Appl. Phys. Lett. **39**, 280 (1981).
15. P. N. Dmitriev, I. L. Lapitskaya, L. V. Filippenko, A. B. Ermakov, S. V. Shitov, G. V. Prokopenko, and V. P. Koshelets, IEEE Trans. Appl. Supercond. **13**, 107 (2003).
16. K. I. Rudakov, P. N. Dmitriev, A. M. Baryshev, A. Khudchenko, R. Hesperand, and V. P. Koshelets, Izv. Vyssh. Uchebn. Zaved., Radiofiz. **62** (7–8), 613 (2019).
17. T. Imamura and S. Hasuo, IEEE Trans. Appl. Supercond. **2**, (1992).
18. L. V. Filippenko, S. V. Shitov, P. N. Dmitriev, A. B. Ermakov, V. P. Koshelets, and J. R. Gao, IEEE Trans. Appl. Supercond. **11**, 816 (2001).
19. P. N. Dmitriev, Cand. Sci. (Phys. Math.) Dissertation (Kotel'nikov Inst. Radioelectron. RAS, Moscow, 2009).
20. L. V. Filippenko, Cand. Sci. (Phys. Math.) Dissertation (Kotel'nikov Inst. Radioelectron. RAS, Moscow, 2009).
21. G. de Lange, D. Boersma, J. Dercksen, P. Dmitriev, A. B. Ermakov, L. V. Filippenko, H. Golstein, W. M. Ruud, L. de Jong Hoogeveen, A. V. Khudchenko, N. V. Kinev, O. S. Kiselev, B. van Kuik, A. de Lange, J. van Rantwijk, A. S. Sobolev, M. Yu. Torgashin, E. Vries, P. A. Yagoubov, and V. P. Koshelets, Supercond. Sci. Technol. **23**, 045016 (2010).
22. V. P. Koshelets, P. N. Dmitriev, M. I. Faley, L. V. Filippenko, K. V. Kalashnikov, N. V. Kinev, O. S. Kiselev, A. A. Artanov, K. I. Rudakov, A. de Lange, G. de Lange, V. L. Vaks, M. Y. Li, and H. Wang, IEEE Trans. THz Sci. Technol. **5**, 687 (2015).
23. N. V. Kinev, K. I. Rudakov, L. V. Filippenko, A. M. Baryshev, and V. P. Koshelets, J. Appl. Phys. **125**, 151603 (2019).
24. N. V. Kinev, K. I. Rudakov, L. V. Filippenko, A. M. Baryshev, and V. P. Koshelets, IEEE Trans. THz Sci. Technol. **9**, 557 (2019).
25. J. G. Simmons, J. Appl. Phys. **34**, 1793 (1963).
26. W. F. Brinkman, R. C. Dynes, and J. M. Rowell, J. Appl. Phys. **41**, 1915 (1970).
27. L. P. Bulat, V. V. Konopel'ko, and D. A. Pshenai-Severin, Vestn. Mezhdun. Akad. Kholoda, No. 3, 46 (2013).
28. M. E. Paramonov, L. V. Filippenko, P. N. Dmitriev, M. Yu. Fominsky, and V. P. Koshelets, J. Commun. Technol. Electron. **64**, 1144 (2019).
29. J. M. Rowell, W. L. McMillan, and W. L. Feldmann, Phys. Rev. **180**, 658 (1969).

*Translated by Yu. Ryzhkov*